Published in final edited form as:
Inorg Chem. 2012 February 20; 51(4): 2338–2348. doi:10.1021/ic202329y.

Mixed-Valence Nickel-Iron Dithiolate Models of the [NiFe]-Hydrogenase Active Site

David Schilter[a], **Mark J. Nilges**[a], **Mrinmoy Chakrabarti**[b], **Paul A. Lindahl**[b], **Thomas B. Rauchfuss**[a], and **Matthias Stein**[c]

[a]Department of Chemistry, University of Illinois, 600 S. Goodwin Ave. Urbana, IL 61801

[b]Department of Chemistry, Texas A&M University, College Station, TX 77842-3012

[c]Max Planck Institute for Dynamics of Complex Technical Systems, Sandtorstraβe 1, 39106 Magdeburg, Germany

Abstract

A series of mixed-valence iron-nickel dithiolates is described. Oxidation of (diphosphine)Ni(dithiolate)$Fe(CO)_3$ complexes **1**, **2**, and **3** with ferrocenium salts affords the corresponding tricarbonyl cations $[(dppe)Ni(pdt)Fe(CO)_3]^+$ ($[\mathbf{1}]^+$), $[(dppe)Ni(edt)Fe(CO)_3]^+$ ($[\mathbf{2}]^+$) and $[(dcpe)Ni(pdt)Fe(CO)_3]^+$ ($[\mathbf{3}]^+$), respectively, where dppe = $Ph_2PCH_2CH_2PPh_2$, dcpe = $Cy_2PCH_2CH_2PCy_2$, $pdtH_2$ = $HSCH_2CH_2CH_2SH$ and $edtH_2$ = $HSCH_2CH_2SH$. The cation $[\mathbf{2}]^+$ proved unstable, but the propanedithiolates are robust. IR and EPR spectroscopic measurements indicate that these species exist as C_s-symmetric species. Crystallographic characterization of $[\mathbf{3}]BF_4$ shows that Ni is square planar. Interaction of $[\mathbf{1}]BF_4$ with *P*-donor ligands (L) afforded a series of substituted derivatives of type $[(dppe)Ni(pdt)Fe(CO)_2L]BF_4$ for L = $P(OPh)_3$ ($[\mathbf{4a}]BF_4$), $P(p\text{-}C_6H_4Cl)_3$ ($[\mathbf{4b}]BF_4$), PPh_2(2-py) ($[\mathbf{4c}]BF_4$), $PPh_2(OEt)$ ($[\mathbf{4d}]BF_4$), PPh_3 ($[\mathbf{4e}]BF_4$), $PPh_2(o\text{-}C_6H_4OMe)$ ($[\mathbf{4f}]BF_4$), $PPh_2(o\text{-}C_6H_4OCH_2OMe)$ ($[\mathbf{4g}]BF_4$), $P(p\text{-tol})_3$ ($[\mathbf{4h}]BF_4$), $P(p\text{-}C_6H_4OMe)_3$ ($[\mathbf{4i}]BF_4$), $PMePh_2$ ($[\mathbf{4j}]BF_4$). EPR analysis indicates that ethanedithiolate $[\mathbf{2}]^+$ exists as a single species at 110 K, whereas the propanedithiolate cations exist as a mixture of two conformers, which are proposed to be related through a flip of the chelate ring. Mössbauer spectra of **1** and oxidized *S* = ½ $[\mathbf{4e}]BF_4$ are both consistent with a low-spin Fe(I) state. The hyperfine coupling tensor of $[\mathbf{4e}]BF_4$ has a small isotropic component and significant anisotropy. DFT calculations using the BP86, B3LYP, and PBE0 exchange-correlation functionals agree with the structural and spectroscopic data, suggesting that the SOMOs in complexes of the present type are localized in a Fe(I)-centered $d(z^2)$ orbital. The DFT calculations allow an assignment of oxidation states of the metals and rationalization of the conformers detected by EPR spectroscopy. Treatment of $[\mathbf{1}]^+$ with CN^- and compact basic phosphines results in complex reactions. With dppe, $[\mathbf{1}]^+$ undergoes quasi-disproportionation to give **1** and the diamagnetic complex $[(dppe)Ni(pdt)Fe(CO)_2(dppe)]^{2+}$ ($[\mathbf{5}]^{2+}$), which features square-planar Ni linked to an octahedral Fe center.

Introduction

The modeling of the active sites of the hydrogenases (H_2ases) is fertile area for research because the inorganic chemistry at play is unusual. Most distinctive is the prevalence of paramagnetic states; this contrasts the chemistry of metal carbonyls in which open shell species are uncommon. Why have H_2ases adopted *S* = ½ states, especially given that the H_2/H^+ redox process involves $2e^-$? While good progress has been made on modeling the paramagnetic states of the [FeFe]-H_2ases,[1-3] synthetic models for the corresponding odd-electron states of the [NiFe]-H_2ases have not been characterized as well.

The active sites of [NiFe]-H_2ases exist in several *S* = ½ states, but only the Ni-C state (Scheme 1)[4] is implicated in the catalytic mechanism.[5,5] Spectroscopic analysis of the Ni-C

state indicates a Ni(III)Fe(II) center bridged by a hydrido ligand.[6,7] Upon irradiation at low-temperatures, Ni-C converts to Ni-L (Scheme 2), another $S = ½$ state first observed in enzymes from *A. vinosum*.[8] Spectroscopic analysis and DFT calculations indicate a Ni(I)Fe(II) core in which the hydrido bridge is absent. Thus, Ni-C undergoes a photoreduction in which the two-electron more reduced Ni-L is reached. Photoconversion appears to involve the deprotonation of Ni-C by a proximal base which has not been identified.[9] EPR and ENDOR experiments and DFT calculations on the Ni-L state have shown that the majority of the unpaired spin density is localized at the Ni atom, consistent with a Ni(I)Fe(II) oxidation state assignment.

Ni-A (unready) and Ni-B (ready) are more oxidized $S = ½$ states of H_2ases, both with Ni(III)Fe(II) cores. High resolution crystallographic studies have been reported for the enzymes from *Desulfovibrio gigas* (85% Ni-A/15% Ni-B),[10]*Desulfovibrio fructosovurans* (Ni-B),[11]*Desulfovibrio vulgaris* Miyazaki F (Ni-B,[12] Ni-SI/Ni-R),[13] and *Desulfovibrio desulfuricans* (Ni-B).[14] Regardless of the state of the enzyme, the active site consists of Ni coordinated to four thiolato (or thiol) ligands, two of which bridge to an 'organometallic' $Fe(CN)_2(CO)$ fragment.[15] Although the first [NiFe]-H_2ase crystal structure appeared in 1993, synthetic modeling of this family of hydrogenases has only recently afforded complexes whose structures approach this active site.

Synthetic models featuring a NiFe core, in which Ni(II) is bound by four sulfur ligands have been reported by the Tatsumi group (Figure 1, left).[16] This dithiocarbamato complex, in addition to reproducing the Ni coordination environment, also features the $Fe(CN)_2(CO)$ fragment, albeit bound to a thioether. The CN and CO bands in the IR spectrum match those of the enzyme in the unready Ni-A state, suggesting that the Fe(II) centers in the model complex and [NiFe]-H_2ase have similar electron densities. Complexes of this type may be considered models for Ni-SCO, an EPR-silent H^--free state of [NiFe]-H_2ase in which the Ni and Fe centers are in the + II oxidation state, the latter being octahedrally coordinated.

Jiang and co-workers have prepared a related Ni(II)Fe(II) structural model (Figure 1, right), which incorporates a $Fe(CN)_2(CO)_2$ fragment bridged to Ni by a pair of thiolate ligands.[17] This complex is closely related to the dithiocarbamate example, although an additional CO replaces the thioether at the Fe(II) center and the chelating diphosphine dppe is used in place of the dithiocarbamate. Dppe has also been employed as a surrogate for terminal thiolates in [(dppe)Ni(pdt)$Fe(CO)_3$] (**1**), a model described by Schröder and co-workers.[18] In contrast to the models discussed above, the Fe center is bound to only three ligands besides the bridging thiolates. This derivative features metal-metal bonding absent in more oxidized NiFe complexes such as those described by Tatsumi, Jiang, and their co-workers.

The formally Ni(I)Fe(I) species **1** readily protonates to furnish the conjugate acid [(dppe)Ni(pdt)(μ-H)$Fe(CO)_3$]BF_4 ([**1**H]BF_4), which features a hydrido ligand bridging the Ni(II) and Fe(II) centers.[19] This complex was the first hydride of a NiFe thiolate, and the significance of this stoichiometric resemblance is enhanced by this complex's ability to catalyze the reduction of protons to H_2. More recently, the Fe coordination sphere has been varied to afford more electron-rich derivatives of type [(dppe)Ni(pdt)(μ-H)$Fe(CO)_2(PR_3)]^+$.[20] This family of hydrido complexes represent promising models for the Ni-R state of [NiFe]-H_2ase, which is characterized by an $S = 0$ Ni(II)Fe(II) core with a proposed bridging hydrido ligand.

In a preliminary communication, we reported that oxidation of the neutral complex **1**[20] using a ferrocenium salt ($FcBF_4$) allowed for the *in situ* preparation of [(dppe)Ni(pdt)$Fe(CO)_3$]BF_4 ([**1**]BF_4), which was characterized by IR and EPR spectroscopy.[19] This salt remains the only potential mimic of a paramagnetic state of the

enzyme. In this paper we describe the synthesis of a series of $S = ½$ NiFe carbonyls, the first models for Ni-L. Such compounds have spin distributions inverse to that of Ni-L, and their characterization sheds new light on the role of the ligands in fine-tuning electronic structure of bimetallic species. Additionally, our studies revealed the tendency of some members of this series to undergo disproportionation, thereby affording potential models for Ni-SCO state.

Results

[(diphosphine)Ni(pdt)Fe(CO)$_3$]$^+$

Preliminary studies revealed that (dppe)Ni(pdt)Fe(CO) $_3$(**1**) and related complexes undergo oxidation at ~ -0.5 V *vs*. $Fc^{+/0}$. For this reason, the new cations were prepared from the neutral Ni(I)Fe(I) complexes and $FcBF_4$. The first example of the series is [**1**]BF_4, which could be isolated as a brown powder. This salt dissolves in CH_2Cl_2 to give moderately stable solutions, which are unaffected by ambient light but are sensitive to O_2 and H_2O. Solutions in THF and MeCN decompose to unidentified products. Using the appropriate ferrocenium salts, we also prepared solutions of [**1**]$BAr^F{}_4$ ($BAr^F{}_4^-$ = tetrakis(3,5-bis(trifluoromethyl)phenyl)borate) and [**1**]PF_6. The latter could be isolated as a brown powder. Although the solubility properties of these salts varied, their IR and EPR spectra (see below) were very similar.

Under ^{13}CO (1 atm), **1** in CH_2Cl_2 solution converted to [(dppe)Ni(pdt)Fe($^{13}CO)_3$] (**1′**), for which the ν_{CO} bands are shifted to lower energies (1982 (m), 1913 (s) cm^{-1} *vs*. 2028 (m) , 1932 (s) cm^{-1}). Similarly, [**1**]BF_4 also exchanges with ^{13}CO, allowing for the generation of [(dppe)Ni(pdt)Fe($^{13}CO)_3$]BF_4 ([**1′**]BF_4), which has ν_{CO} bands consistent with complete labeling (2009 (m), 1941 (s) cm^{-1} vs 2057 (m), 1986 (s) cm^{-1}). Analogously to the parent complex, the labeled salt can also be prepared by the oxidation of [(dppe)Ni(pdt)Fe($^{13}CO)_3$] (**1′**) with $FcBF_4$.

The X-band EPR spectrum of a frozen CH_2Cl_2/PhMe solution of [**1**]BF_4 (Figure 2, exp.) exhibits two comparably intense signals, including an axial signal (A) and rhombic signal (B). These signals are consistent with the presence of two isomers. The absence of any ^{31}P hyperfine coupling suggests that negligible spin density resides on the Ni center, suggesting a Fe(I)Ni(II) oxidation state. This was further confirmed by comparing this spectrum to that of the ^{13}CO-labeled compound [**1′**]BF_4 (exp.′). The EPR spectrum of the latter again suggests the presence of two closely related isomers with signals split by a single $I = ½$ nucleus, proposed to be the apical ^{13}C atom. One signal was further split/broadened (A = 13, 30, 17 MHz) owing to weak interactions with the two equivalent basal ^{13}CO ligands. For comparison, the coupling observed for the Fe(I)-^{13}CO spin system in the H_{ox} state of [FeFe]-H_2ase is 21 MHz.[21] EPR spectra for [**1**]BF_4, [**1**]PF_6, and [**1**]$BAr^F{}_4$ were similar.

Two analogs of [**1**]$^+$ were examined involving replacement of the dithiolate and the diphosphine. Oxidation of ethanedithiolate [(dppe)Ni(edt)Fe(CO)$_3$] (**2**)[22] with ferrocenium salts gave unstable products regardless of the counteranion. *In situ* IR analysis of these solutions confirmed that the cation [**2**]$^+$ (ν_{CO} = 2059 (m), 1988 (s) cm^{-1}) closely resembles [**1**]$^+$, although these solutions also contained significant amounts of **2** and [**2**H]$^+$. The instability of [**2**]$^+$ contrasts with the good stability of the corresponding hydrido complex [**2**H]$^+$, whose structure is expected to closely resemble that of the mixed-valence derivative. The EPR analyses of [**2**]$^+$ are discussed later. Lastly, oxidation of the more electron-rich complex [(dcpe)Ni(pdt)Fe(CO)$_3$] (**3**) with $FcBF_4$ in CH_2Cl_2 solution afforded [**3**]BF_4, which is similar to [**1**]BF_4 in terms of its spectroscopy (Figures S14, S15) and stability.

Structure of [(dcpe)Ni(pdt)Fe(CO)$_3$]BF$_4$

X-ray crystallography allowed for structural confirmation of [**3**]BF_4, the results of which are presented in Figure 3.

The Ni-Fe distance in [**3**]BF_4 (2.818 Å) is longer than that in **1** (2.467 Å) as well as the Ni(II) (μ-H)Fe(II) complex [**3**H]BF_4 (2.684 Å), in which a hydrido ligand is present. While the atom connectivity in **3** and [**3**]$^+$ is identical, a dramatic conformational change occurs upon oxidation. The Ni center in [**3**]BF_4 exists in an almost square planar coordination environment, as indicated by the twist angle of 3.55° between the NiP_2 and NiS_2 planes (c.f. 84.91° for the pseudo-tetrahedral Ni center in **1**).[18] By comparison, the (dcpe)Ni(pdt) fragment in [**3**H]BF_4 is also almost square planar, and the average Ni-P distance for this complex (2.189 Å) is identical to that in [**3**]BF_4.[20] The solid state data are consistent with [**3**]BF_4 featuring a Ni(II) center. The Fe center is situated in an approximately square-pyramidal $S_2P(CO)_2$ environment, a geometry often adopted by mononuclear Fe(I)[23] and dinuclear Fe(I)Fe(II) compounds.[24,25] The Fe-C_{basal} distances (1.799, 1.790 Å) are somewhat shorter than the Fe-C_{apical} distance (1.833 Å), as might be expected for a complex with CO ligands *trans* to strong σ-donors. Furthermore, the average Fe-C distance in [**3**]BF_4 (1.807 Å) is similar to that for **1** (1.798 Å), consistent with the Fe centers in both complexes being in the same (+I) oxidation state.

Substituted Derivatives of [1]$^+$

In an attempt to introduce CN^- ligands, a solution of [**1**]$B(3,5\text{-}(CF_3)_2C_6H_3)_4$ was treated with NBu_4CN. However, this reaction afforded **1** as the predominant species according to IR analysis. The redox process was rapid and accompanied by effervescence, believed to result from evolution of NCCN. The formation of **1** was also observed when [**1**]BF_4 was treated with either the *N*-heterocyclic carbene bis(2,6-diisopropylphenyl)imidazolin-2-ylidene or the isocyanide MeNC.

Given the propensity of *C*-donors to reduce [**1**]$^+$, less basic ligands were investigated. Addition of [**1**]BF_4 to an excess of PPh_3 in CH_2Cl_2 solution resulted in effervescence (evolution of CO) and formation of a dark red-brown solution. The reaction was instantaneous, and a red-brown powder could be precipitated with pentane. The IR spectrum of this product features a pair of comparably intense ν_{CO} bands at 1988 and 1929 cm^{-1}, consistent with the formation of the monosubstituted *cis*-dicarbonyl species [(dppe)Ni(pdt)Fe(CO)$_2$PPh$_3$]BF_4 ([**4e**]BF_4) according to Scheme 4. The mean shift in ν_{CO} upon substitution is -63 cm^{-1} relative to the tricarbonyl parent compound [**1**]BF_4 (ν_{CO} = 2057, 1986 cm^{-1}). An identical shift in ν_{CO} was observed upon replacement of one CO for PPh_3 in [**1**H]BF_4 to give [(dppe)Ni(pdt)(μ-H)Fe(CO)$_2$PPh$_3$]BF_4.[26] Further information regarding the identity of [**4e**]BF_4 was gleaned from its positive-ion ESI mass spectrum, which featured a base peak at *m/z* 936.3 for the parent ion [**4e**]$^+$.

Analogous to the preparation of [**4e**]BF_4, a range of other monosubstituted derivatives were prepared ([**4a-j**]BF_4), each of which was characterized according to analytical and ESI-MS data, as well as by IR and EPR spectroscopy. ESI-MS analyses supported the formulation of the new complexes as [(dppe)Ni(pdt)Fe(CO)$_2$L]$^+$. Ionization by loss of BF_4^- from the salts allowed for the detection of the parent ions, with the isotopic distributions being consistent with their structures. In some cases significant fragmentation was also observed, in which the cations lose a terminal ligand to afford species of the type [(diphosphine)Ni(dithiolate)Fe(CO)$_2$]$^+$ and [(dppe)Ni(pdt)Fe(CO)L]$^+$.

The ν_{CO} values for the compounds prepared are given in Table 1. These data correlate inversely with the basicity of the monodentate *P*-donor ligands employed. As expected, the trend in ν_{CO} values roughly mirrors the trend in the Tolman Electronic Parameter[27] (TEP)

for each *P*-donor ligand. The similarity of the IR data for complexes of PPh_3, PPh_2(2-py) ([**4c**]BF_4), PPh_2(*o*-C_6H_4OMe) ([**4f**]BF_4), and PPh_2(*o*-$C_6H_4OCH_2OMe$) ([**4g**]BF_4) indicates that ether and pyridyl substituents do not interact significantly with the metal centers in the monocations.

In many cases the two ν_{CO} bands have discernable shoulders at lower energy, suggesting that the complexes are present as two species in solution. This is most pronounced in the case of the $PMePh_2$ complex ([**4j**]BF_4), where the absorptions can be somewhat resolved (Figure S48). The isomerism involved is addressed in the following section.

EPR spectroscopy of [(dppe)Ni(pdt)Fe(CO)$_2$L]$^+$

All substituted mixed-valence derivatives were characterized by X-band EPR spectroscopy; selected spectra were simulated in order to extract *g* and *A*(^{31}P) values, which are presented in Table 2. Spectra not presented here can be found in the SI.

The EPR spectrum of the PPh_3-containing compound [**4e**]BF_4 features a pattern of two overlapping rhombic signals, consistent with the lower symmetry of [**4e**]$^+$ relative to [**1**]$^+$. The hyperfine splitting of the signals is attributed to the coupling to the PPh_3 ligand, the associated *A* values being in the range 117 – 217 MHz. Spectra for [**4a-j**]BF_4 are similar. BP/TZP calculations predict a large isotropic hyperfine coupling of +202 MHz for $^{31}\underline{P}Ph_3$ in [**4e**]$^+$ and a dipolar contribution of (-17, -16, +33) MHz . The hyperfine coupling to the dppe P nuclei is significantly weaker (A_{iso} = 4 MHz).

The ^{13}CO-labeled derivative [(dppe)Ni(pdt)Fe(^{13}CO)$_2$$PPh_3$]$BF_4$ ([**4e′**]BF_4, prepared from [**1′**]), was studied in order to derive further structural information about complexes of the present type. In their EPR spectra, the *g*-values for [**4e**]BF_4 and [**4e′**]BF_4 are identical (Table 2). In addition to the ^{31}P coupling arising from Fe-bound PPh_3, further signal broadening is observed in the case of [**4e′**]BF_4, a result of weak interactions with the two ^{13}CO ligands (Figure S35). This might suggest that in such arrangements a ligand must be in the apical position to interact strongly with the Fe-centered SOMO.

The compound [**4a**]BF_4 is noteworthy owing to its high A_P values, which average 354 and 345 MHz for the axial and rhombic components (2:1), respectively (Figure 5). These values suggest significant spin delocalization onto the $P(OPh)_3$ ligand, which is the best π-acceptor of the *P*-donor ligands employed. The ^{13}CO-labeled compound [**4a′**]BF_4 was prepared to clarify the assignment. As with the PPh_3 congener [**4e′**]BF_4, the presence of ^{13}CO ligands results in only slight signal broadening, suggesting that the $P(OPh)_3$ ligand is apically bound to Fe(I), with the ^{13}CO ligands occupying the basal positions.

EPR spectra of the Ni(II)Fe(I) compounds [**1**]BF_4, [**3**]BF_4 and [**4a-j**]BF_4 (and the ^{13}CO-labeled analogs prepared) indicate, in each case, the presence of two species. For [**4aj**]BF_4 these isomers have almost identical EPR parameters. Indeed, satisfactory simulations could only be obtained when two species were considered. It is suggested that these species are very similar, and the data are consistent with the isomers being related by a ring flip of the bridging pdt^{2-} ligand (Scheme 5). The presence of two isomers is more pronounced when the room temperature spectra are considered (selected spectra presented in SI), suggesting a slow interconversion between conformers (‘flipamers’). Additionally, the dispersion afforded by Q-band EPR was exploited in the analysis of one example, [**4e**]BF_4. In this case the high field (g_z) resonance has obvious shoulders which are evident in one of the two modeled signals (Figure 32, SI).

The existence of flipamers is found in pdt-bridged dinuclear species, the ring inversion/flipping barriers typically being 8-11 kcal/mol.[28,29] For example, EPR spectroscopy was

used to detect the two flipamers of the [FeFe]-H_2ase model complex [(dppv)(CO)Fe(pdt)Fe$(CO)_2(PMe_3)$]$^+$ (dppv = *cis*-1,2-bis(diphenylphosphino)ethene).[24]

This isomerism is not possible for the ethanedithiolate cation [**2**]$^+$, and although it was too unstable to be isolated as a salt, EPR analysis was conducted on a sample prepared *in situ*. The spectrum recorded at 110 K (Figure 5) an almost purely axial signal, corresponding to a single spin system. The signal at higher field is split into a triplet, whereas the hyperfine splitting of the low-field resonance is unresolved.

A rhombic EPR spectrum was observed at room temperature, again implying the presence of a single species in which an unpaired electron is coupled to two equivalent I = ½ nuclei. Such a signal arises either from the coupling of an Fe(I) center with two protons on the edt^{2-} ligand or a Ni(I)-^{31}P interaction; this question is addressed in the following section. The fact that this complex is present as a single species in solution is consistent with the two EPR signals from [**1**]BF_4 arising from the presence of flipamers.

DFT Calculations

Density functional theoretical calculations were performed in an effort to rationalize EPR data and assign the oxidation states. The calculations support the assignments of Ni(I)Fe(I) for the neutral complexes and Ni(II)Fe(I) for the singly oxidized derivatives. The calculated structural parameters agree with those determined experimentally to within 0.01 Å for bond lengths and 1-2° for bond angles. The structure calculated for [**1**]$^+$ (Figure 7) is very similar to that observed crystallographically for [**1**]$^+$, with the Ni-Fe distances being 2.818 Å and 2.80 Å, respectively.

With the observed structure, the Mulliken population of the unpaired spin on Fe is 0.72 and on Ni is 0.12 (see Figure 7). Upon ring inversion pdt^{2-} chelate ring, the distribution of the unpaired spin density remains nearly unchanged, but small differences in *g*-values are detectable (*vide infra*).

The calculated *g*-tensor principal values from the spin-unrestricted Orca calculations and spin-restricted ZORA calculations give a consistent picture of the electronic structure of the mixed-valence NiFe dithiolates. The *g*-values reported for Ni-L (2.30, 2.12, 2.05), in particular the deviation of the g_z component from g_e (2.0023), are indicative of the presence of Ni(I) in this state of the enzyme. Calculations using the BP86 (Becke exchange, Perdew correlation),[30,31] B3LYP (Becke exchange, Lee-Yang-Parr correlation)[32] and PBE0 (Perdew, Burke and Ernzerhof)[33,34] hybrid functionals give *g*tensors for the compounds [**1**]$^+$, [**2**]$^+$, [**3**]$^+$, [**4a**]$^+$ and [**4e**]$^+$ (Table 1, SI) in which the smallest *g*-component g_3 is close to g_e, effectively ruling out Ni(I) species.

In general BP86 tends to underestimate *g*-shifts by about 19 ppt for g_1, whereas PBE0 tends to slightly overestimate *g*-shifts. Best agreement with experiment is obtained with the B3LYP hybrid functional. The self-consistent consideration of spin-orbit coupling in spin-restricted calculations with Slater basis functions gives larger *g*-shifts compared to the effective potential approach through the coupled-perturbed SCF equation. The calculations are accurate enough to assign the two conformers (see Scheme 5). For example, the experimental *g*-tensors for [**1**$^+$] (2.052, 2.050, 2.005 and 2.055, 2.038, 2.009) can be compared to those derived computationally (ZORA, B3LYP). Calculations suggest that axial *g*-values (2.052, 2.051, 2.006) can be expected when the central CH_2 is oriented toward Ni (flipamer 'a'). Slightly lower *g*-values can be observed (2.051, 2.047, 2.005) when this group is instead closer to Fe (as it is in flipamer 'b'). Whereas g_1 remains almost unchanged, the largest decrease occurs for g_2. This can be rationalized by the g_2-axis pointing towards thiolate bridging ligand and is thus sensitive to the orientation of the pdt

ligand. In two cases, the relative energies between flipamers and their barrier to interconversion were computed. For the tricarbonyl complex [**1**]$^+$, the Gibbs free energy of flipamer 'a' is lower by 1 kcal/mol, the activation barrier for conversion to flipamer 'b' being 9 kcal/mol. The flipamers of the PPh_3-substituted derivative [**4e**]$^+$ are almost isoenergetic: flipamer 'b' is favored by 0.2 kcal/mol, the barrier being 10.5 kcal/mol. The calculated barriers are comparable to those reported for diiron propanedithiolates (*vide supra*) and are consistent with the observation of two species by EPR spectroscopy. Of course, such a treatment is not applicable for the ethanedithiolate complex [**2**]$^+$, the EPR spectrum of which can be modeled using a single conformer.

The calculated atomic spin densities show that the majority of the unpaired spin (0.7 - 0.9e$^-$) resides on the Fe atom (Table 3). The Ni center only carries about 0.03 - 0.12 e$^-$. According to these calculations, the conformation of the pdt ring has little influence on the spin density distribution and thus on the hyperfine interactions. The ^{31}P nuclei of the bidentate dppe and dcpe ligands give rise to only small hyperfine interactions with isotropic components each between -4 and -15 MHz.

The apical ligand on the Fe atom can acquire about 5% of the unpaired spin density. This results in an almost isotropic ^{13}C hyperfine interaction ranging +69 to +76 MHz for [**1**]$^+$ and [**2**]$^+$ with a small dipolar contribution (-5, -3, +8 MHz). The hyperfine couplings to the other two ^{13}CO ligands are significantly smaller (-16, -17 MHz) and cannot be resolved in the experimental EPR spectra. In [**4e**]$^+$ there exists a large isotropic hyperfine interaction (+178 and +204 MHz for the two conformers) with the $^{31}PPh_3$ ligand in addition to a small dipolar component (-18, -16, +34 MHz).

Mössbauer Spectra

The neutral complex **1** and the mixed-valence species [**4e**]BF_4, [**4h**]BF_4, and [**4i**]BF_4 were studied by Mössbauer spectroscopy. At 6 K and 0.05 T applied field, **1** exhibited a quadrupole doublet (δ = 0.04 mm/s and E_Q = 0.68 mm/s), consistent with a diamagnetic complex containing low-spin Fe(I). Under similar conditions, analysis of the diiron(I) species $(CO)_3Fe(pdt)Fe(CO)_3$ yielded the parameters δ = 0.04 mm/s and ΔE_Q = 0.77 mm/s (Figure S52). These data further highlight the parallels between these two low-spin Fe(I) metal-metal bonded derivatives.

Surprisingly, the one-electron oxidized S = ½ complexes [**4e**]BF_4, [**4h**]BF_4, [**4i**]BF_4 in the solid state also exhibited a quadrupole doublet at 6 K and 0.05 T. This appeared to be inconsistent with the EPR and DFT studies (*vide supra*), which indicated unpaired spin density on these complexes, primarily on the Fe (Figure 8). In such cases, it was expected that paramagnetic hyperfine structure would be observed under the experimental conditions employed.

It was reasoned that the apparent inconsistency could be due to intermolecular spin-spin interactions. Accordingly, [**4e**]BF_4 was studied at 4.3 K in a strong applied magnetic field (6 T), where these interactions would be less apparent. Indeed, the high field data indicated the presence of magnetic hyperfine interactions which prompted us to examine a frozen solution of [**4e**]BF_4 (5 mM, CH_2Cl_2/PhMe, 1 : 2). At 6 K and 0.05 T applied field, the Mössbauer spectrum of the solution indicated the presence of magnetic hyperfine interactions. Such low concentrations circumvented spin-spin interactions but resulted in noisy spectra. Analysis of a more concentrated sample (40 mM) afforded a similar low field, low temperature spectrum but with higher S/N (Figure S53). Indeed, data collected at applied fields of 4 and 6 T were, apart from the poorer S/N, indistinguishable from those of solid [**4e**]BF_4. The low field spectrum of this frozen solution and the high temperature, high field data of the solid sample could be simulated with an S = ½ Hamiltonian (Figure 9, parameters in caption). The

calculated Mössbauer parameters of η = 0.8 and a NQCC of 11 MHz agree well with those measured. The ^{57}Fe hyperfine tensor for [**4e**]BF_4 has a small isotopic component, A_{iso} = (A_x+ A_y+ A_z)/3 = -9.1 MHz and significant anisotropy. The calculated ^{57}Fe isotropic hyperfine coupling parameters (A_{iso} = -4 MHz, SR UKS ZORA B3LYP/TZP and A_{iso} = -1.5 MHz for SR UKS ZORA BP/TZP) and larger anisotropic hyperfine tensors (SR UKS B3LYP/TZP (-22, -10, +32) MHz and SR UKS BP/TZP (-18, -9, +27) MHz) are in good agreement with those measured.

Disproportionation Reactions

Interaction of [**1**]$^+$ with small basic phosphine ligands results in complicated mixtures. For example, addition of [**1**]$^+$ to excess PBu_3 in CH_2Cl_2 induces a 'disproportionation' reaction affording **1** and a product formulated as [(dppe)Ni(pdt)Fe(CO)$_2$(PBu_3)$_2$](BF_4)$_2$. Precipitation of the latter compound allowed for its identification according to ESI-MS (*m/z* 1166.1 [M – BF_4^-]$^+$, 539.5 [M – 2BF_4^-]$^{2+}$) and ^{31}P NMR (60 (dppe), 28 (PBu_3) ppm) data. A strong ν_{CO} band could be observed at 1965 cm^{-1}, with a weaker one at 2037 cm^{-1}. Along with the NMR data, these data indicate the presence of a Fe(II)(CO)$_2$(PBu_3)$_2$ fragment in which the CO ligands are mutually trans, although other isomers could be present. Similar products were observed when PMe_3 (ν_{CO} 1971 cm^{-1}, *m/z* 913.5 [M – BF_4^-]$^+$, 413.6 [M – 2BF_4^-]$^{2+}$) and PMe_2Ph (ν_{CO} 1971 cm^{-1},*m/z* 1037.5 [M – BF_4^-]$^+$, 475.3 [M – 2BF_4^-]$^{2+}$) were employed in place of PBu_3. Overall, these data suggest that a disporportionation-type reaction is triggered when a sufficiently small pair of ligands bind Fe.

More tractable products of disproportionation were obtained when the diphosphine dppe was used. At room temperature, a rapid reaction was indicated by IR spectroscopy; the products are **1** and the new salt formulated as [(dppe)Ni(pdt)Fe(CO)$_2$(dppe)](BF_4)$_2$ ([**5**](BF_4)$_2$ (Scheme 6).

This compound can be prepared in good yield by treatment of a CH_2Cl_2 solution of **1** and $FcBF_4$ (2 equiv.) with dppe. On the basis of its ^{1}H and ^{31}P NMR spectra, [**5**]$^{2+}$ is diamagnetic and symmetrical in CD_2Cl_2 solution. Further evidence supporting the proposed structure could be obtained by ESI-MS, which allowed for the detection of ions at *m/z* 1158.7 and 536.1, assigned to {[**5**]BF_4}$^+$ and [**5**]$^{2+}$, respectively.

Structure of [(dppe)Ni(pdt)Fe(CO)$_2$(dppe)](BF_4)$_2$

The solid state structure of [**5**]$^{2+}$ was established by X-ray crystallography (Figure 10).

As expected, the complex dication features a pdt^{2-} ligand bridging the Ni and Fe centers, which exist in square planar and octahedral ligand environments, respectively. These coordination geometries, and a Ni-Fe distance of 3.203 Å, are reflective of a Ni(II)Fe(II) complex lacking a metal-metal bond. The Fe-C distances (1.800, 1.817 Å) are similar, and this solid state data are corroborated by the IR solution spectrum, which features a single CO band (1975 cm^{-1}), consistent with the presence of two *trans* CO ligands. Indeed, the complex is roughly symmetric, as evidenced by the two Fe-S (2.325, 2.334 Å), Ni-P (2.180, 2.186 Å) and Ni-S (2.219, 2.253 Å) bonds of similar pairwise lengths. These are comparable to the average Ni-P (2.176 Å) and Ni-S (2.222 Å) distances in the related dinickel(II) complex {(pdt)[Ni(dppe)]$_2$}(BF_4)$_2$.[35] The product resembles [(dppe)Ni(pdt)Fe(CO)$_2$(CN)$_2$],[17] and might be compared to the 34e$^-$ Ni(II)Fe(II) core present in the Ni-SCO state of [NiFe]-H_2ase.

Discussion

Oxidation of Ni(I)Fe(I) dithiolates affords mixed-valence derivatives, which are described as Ni(II)Fe(I) species. Several lines of evidence support this assignment: (i) crystallographic

analysis shows that Fe-C bond lengths are unaffected by oxidation of the Ni(I)Fe(I) precursor whereas the Ni coordination geometry changes from being tetrahedral to square planar, (ii) in the EPR spectra of the cations, hyperfine coupling is observed with ^{13}CO (on Fe) but not the diphosphine (on Ni), and (iii) the Mössbauer parameters observed are similar to other Fe(I) sites. Additionally, as has recently been described, the potentials for the oxidation of Ni(dppe) derivative **1** *vs.* the Ni(dcpe) derivative **3** differ strongly ($E_{½}$ = -0.54 and -0.84 V *vs.* Fc/Fc$^+$, respectively).[22]

In view of the electron-rich Fe(CN)$_2$(CO) fragment present in the [NiFe]-H$_2$ase active site, it was of interest to further modify the tricarbonyl cations by introducing donor ligands. It was anticipated that the displacement of one or more of the CO ligands in [**1**]$^+$ with stronger σ-donors would stabilize oxidation states matching those of the Ni-L state of the enzyme (Ni(I)Fe(II)). For example ENDOR measurements on the Ni-A state revealed a small $A(^{57}\text{Fe})$ of 1 MHz and no hyperfine could be resolved for the enzyme in the Ni-B and Ni-C states.[36] However, the substituted complexes [**4a-j**]$^+$ also appear to be Ni(II)Fe(I) derivatives in which the monodentate *P*-donor ligands occupy the apical Fe coordination site. Donor atoms at this site are proposed to interact strongly with the Fe-centered SOMO, as indicated by the observation of strong hyperfine coupling to only a single ^{13}CO center in [**1**′]$^+$. This is further supported by considering the minimal effect that ^{13}CO labeling has on the EPR spectrum of [**4e**]$^+$, suggesting that the (basal) ^{13}CO ligands in this complex are only weakly coupled to the SOMO.

The substituted derivatives [**4a-j**]$^+$ are expected to be approximately isostructural to one another, given the correlation between ν_{CO} and TEP values for the complexes. The apical location of the *P*-donor ligands in these salts contrasts with the structure of the hydride [(dppe)Ni(pdt)(μ-H)Fe(CO)$_2$PPh$_3$]$^+$, in which PPh$_3$ occupies a basal coordination site.[20] The latter conformation is undoubtedly stabilized by the mutually *trans* arrangement of the H$^-$ (strong σ-donor) and CO (π-acceptor) ligands. The stereochemistry at Fe in the new complexes also differs from the enzyme, in which the two strongly σ-donating CN$^-$ ligands occupy the *basal* sites.

Using ^{13}CO labeling, we confirmed that both **1** and [**1**]BF$_4$ rapidly exchange with CO, which may be relevant to the well-known observation that exogenous CO inhibits [NiFe]-H$_2$ase. Binding of CO to Ni-SI$_a$ affords the EPR-silent Ni-SCO and Ni-SCO$_{red}$ states,[37] while Ni-L reacts with CO to give the Ni-CO state.[38] This state is paramagnetic (S = ½) and features CO coordinated to Ni, which, according to EPR data, is in the + I oxidation state.[39] Although no analogous CO adduct of [**1**]BF$_4$ was observed in our work, short-lived CO adducts would explain the facility by which these cations exchange with CO. It appears likely that the exogenous CO ligand would bind the Fe center; a similar adduct with tertiary phosphine ligands would be an intermediate in the conversion of [**1**]BF$_4$ to [**4a-j**]BF$_4$.

There are notable differences between the spectroscopy of the mixed-valence complexes discussed here and data reported for the Ni-L state of [NiFe]-H$_2$ase.[36] Solution IR data for the mixed-valence complexes suggest that the Fe center in each of these derivatives is still electron-poor relative to the enzyme (ν_{CO} = 1911 cm^{-1} for Ni-L state of *D. vulgaris* Miyazaki F).[40] More significantly, the spin in this state is predominantly localized in the Ni $d(x^2\text{-}y^2)$ and $d(z^2)$ orbitals, with the g-values obtained being 2.298, 2.116 and 2.043.[41] These g-values are considerably larger than those found for [**2**]BF$_4$ (2.053, 2.054, 2.010), in which the spin likely resides on the Fe center. It appears that the incorporation of monophosphines into [**1**]$^+$ is insufficient to reverse the Ni(II)Fe(I) oxidation state assignment of [**1**]$^+$. In fact, instead of resembling Ni-L, the data for the new complexes are closer to those for the [2Fe]$_H$ component in the H$_{ox}$ state of [FeFe]-H$_2$ase. In the enzyme isolated from *C. pasteurianum*, this Fe(I)Fe(II) cluster exhibited an EPR signal with g = 2.097, 2.039, 1.999.[42]

Mössbauer spectra of the diamagnetic Ni(I)Fe(I) complex **1** and the closely related one-electron-oxidized $S = ½$ species were collected to give evidence for the description of the latter as Ni(II)Fe(I) species, given that a more delocalized description might have been possible. Most useful in this analysis were the Fe isomer shifts δ, as well as the magnitude and anisotropy of the *A*-tensors. The δ value was found to be slightly greater for [**4e**]BF_4 relative to **1**. This could suggest a degree of oxidation, relative to the Fe(I) state, but could also reflect differences in coordination environment, given that a CO ligand is substituted for PPh_3 in [**4e**]BF_4. Low-spin Fe(II) can be ruled out given that a very low Fe-centered spin density and *A*-values would be expected in such a case. The *A*-tensor of [**4e**]BF_4 is modest but large enough to support a Fe(I) assignment. Popescu and co-workers also required a relatively small A_{iso} value (9.5 MHz) to simulate Mössbauer spectra of the $[2Fe]_H$ component in the H_{ox}-CO state of [FeFe]-H_2ase from *C. pasterurianum*,[43] although the magnetic hyperfine tensors used were isotropic unlike those employed to simulate spectra of [**4e**]BF_4. From DFT studies using the ADF program, Brunold and co-workers calculated highly anisotropic *A* values, including +11, -1, and -27.5 MHz, for the Fe(I) center in H_{ox}.[44] These values are similar in both sign and magnitude to those used in our simulation, indicating that the ^{57}Fe hyperfine tensor for [**4e**]BF_4 is best explained by a low-spin Fe(I) center. This is also corroborated by our DFT calculations which gave an unpaired spin density of $0.85e^-$ at the Fe atom of [**4e**]BF_4. The increase of δ, relative to that of **1**, suggests some degree of oxidation, but other low spin Fe(I) centers with similar δ (= 0.12 mm/s) have been reported.[45] The low spin Fe(I)Fe(II) cluster in H_{ox} from *C. pasterurianum* has $0.1 < \delta < 0.3$ mm/s; in the H_{ox}-CO state from *Desulfovibrio vulgaris* it has $\delta_{1,2} = 0.13, 0.17$ mm/s,[43,46] similar to the δ value associated with the Fe(I) in [**4e**]BF_4.

Summary

The first examples of mixed-valence ($S = ½$) nickel-iron dithiolates have been prepared. Complexes of the type $[(dxpe)Ni(xdt)Fe(CO)_2L]^+$ are characterized as Ni(II)Fe(I) mixed-valence species on the basis of structural and spectroscopic data. The Ni(II)Fe(I) assignment contrasts the Ni(I)Fe(II) core present in the Ni-L state of [NiFe]-H_2ase and is perhaps more related to the Fe(I)Fe(II) fragment in the H_{ox} state of [FeFe]-H_2ase. The crystallographic results highlight the large geometric changes upon oxidation of the Ni(I)Fe(I) precursor, suggesting that stabilization of Ni(I)Fe(II) complexes smay require not just changes in the terminal ligands, but also greater control of the nickel coordination sphere to better match the see-saw geometry observed for the enzyme.

Experimental

Unless otherwise stated, all chemicals were purchased from commercial sources and used as received. PMe_3 was distilled from CaH_2. The compounds **1**[20], **2**, **3**[22] and $PPh_2(o\text{-}C_6H_4OCH_2OCH_3)$[47] were prepared according to the literature methods. All reactions were conducted in an MBraun glovebox equipped with a solvent purification system; the concentrations of O_2 and H_2O in the N_2 atmosphere were less than 1 ppm. The mixed-valence complexes were stored at -28°C. IR spectra of complexes (in CH_2Cl_2) were recorded on a Perkin-Elmer Spectrum 100 FTIR spectrometer. EPR spectra of complexes (~1 mM in CH_2Cl_2/PhMe, 1:1) were recorded on a Varian E-line 12″ Century Series X-band CW spectrometer. ESI-MS data were acquired using a Waters Micromass Quattro II spectrometer. Analytical data were acquired using an Exeter Analytical CE-440 elemental analyzer. UV-vis data were acquired on a Varian Cary 50 Bio spectrophotometer. NMR spectra were recorded at room temperature on a Varian Unity 500 spectrometer. $^{31}P\{^1H\}$ spectra were collected at 500 MHz and chemical shifts are referenced to external 85% H_3PO_4. Crystallographic data were collected using a Siemens SMART diffractometer equipped with a Mo K_α source (λ = 0.71073 Å) and an Apex II detector. Mössbauer spectra

were collected for samples either suspended in mineral oil or dissolved in CH_2Cl_2/PhMe (1:2). Of the instruments used (MS4 WRC and 12CNDT-6T spectrometers, SEE Co., Edina MN), the former allowed data collection at 6 K with 0.05 T field applied parallel to the γ rays, while the latter gave data at 4.3 K with perpendicular fields as high as 6 T. Spectra were analyzed with WMOSS software. Isomer shifts are quoted relative to α-iron at 298 K.

[(dppe)Ni(pdt)Fe(^{13}CO)$_3$] (1′)

1 (21.1 mg, 30.0 μmol) was dissolved in CH_2Cl_2 (5 mL) and the solution frozen with liquid N_2. The reaction vessel was evacuated, the solution placed under ^{13}CO (1 atm) and warmed to room temperature. The mixture was briefly agitated, allowed to stand for 2 h and evaporated to dryness to afford the product as a green powder (quant.). FT-IR: ν_{CO} = 1982, 1913 cm^{-1}. ^{13}C NMR (126 MHz) 209.3 ppm. ^{31}P NMR (202 MHz) 63.5 ppm. Anal. calcd for $C_{29}{}^{13}C_3H_{30}FeNiO_3P_2S_2{\cdot}0.5CH_2Cl_2$: C, 52.14; H, 4.17; N, 0.00. Found: C, 52.41; H, 4.36; N, 0.00.

[(dppe)Ni(pdt)Fe(CO)$_3$]BF$_4$([1]BF$_4$)

1 (14.1 mg, 20.0 μmol) and $FcBF_4$ (5.5 mg, 20.0 μmol) were dissolved in CH_2Cl_2 (2 mL) with rapid stirring. After 1 min, pentane (-28°C, 15 mL) was added and the mixture allowed to stand at -28°C for 10 min. A solid was isolated by filtration, washed with pentane (-28°C, 2 × 2 mL) and dried briefly to afford the product as a brown powder (12.0 mg, 15.2 μmol, 76%).

FT-IR: ν_{CO} = 2057, 1986 cm^{-1}. ESI-MS: *m/z* 702.1 [M – BF_4^-]$^+$. Anal. calcd for $C_{32}H_{30}BF_4FeNiO_3P_2S_2{\cdot}0.5CH_2Cl_2$: C, 46.89; H, 3.75; N, 0.00. Found: C, 46.73; H, 3.85; N, 0.28.

[(dppe)Ni(pdt)Fe(CO)$_3$]PF$_6$([1]PF$_6$)

This salt was prepared analogously to [**1**]BF_4, using $FcPF_6$ in place of $FcBF_4$. Yield: 78%, brown powder.

FT-IR: ν_{CO} = 2057, 1986 cm^{-1}. Anal. calcd for $C_{32}H_{30}F_6FeNiO_3P_3S_2{\cdot}0.25CH_2Cl_2$: C, 44.55; H, 3.54; N, 0.00. Found: C, 44.51; H, 3.61; N, 0.32.

[(dppe)Ni(pdt)Fe(^{13}CO)$_3$]BF$_4$([1′]BF$_4$)

This salt was prepared analogously to [**1**]BF_4, using **1′** as the precursor.

Yield: 78%, yellow-brown powder. FT-IR: ν_{CO} = 2009, 1941 cm^{-1}. Anal. calcd for $C_{32}{}^{13}C_3H_{30}BF_4FeNiO_3P_2S_2{\cdot}0.75CH_2Cl_2$: C, 45.91; H, 3.71; N, 0.00. Found: C, 45.96; H, 3.80; N, 0.00.

[1]BAr$^F_4$

1 (7.0 mg, 10 μmol) and $FcBAr^F_4$ (10.5 mg, 10 μmol) were dissolved in CH_2Cl_2 (1 mL) with rapid stirring. The deep brown solution was used *in situ* for reactivity studies. FT-IR: ν_{CO} = 2057, 1986 cm^{-1}.

[(dppe)Ni(edt)Fe(CO)$_3$]BF$_4$([2]BF$_4$)

2 (6.9 mg, 10.0 μmol) and $FcBF_4$ (2.7 mg, 10.0 μmol) were dissolved in CH_2Cl_2 (1 mL) with rapid stirring. The deep brown solution was used for *in situ* EPR and IR analyses, the latter indicating that significant amounts of the diamagnetic species **2** and [**2**H]BF_4 were present in the crude mixture. The solution was diluted with PhMe for the EPR analysis.

FT-IR: ν_{CO} = 2059, 1988 cm^{-1}. ESI-MS: *m/z* 688.1 $[M - BF_4^-]^+$.

[(dcpe)Ni(pdt)Fe(CO)$_3$]BF$_4$([3]BF$_4$)

This salt was prepared analogously to [**1**]BF_4, using **3** as the precursor. Yield: 78%, brown powder. FT-IR: ν_{CO} = 2054, 1982 cm^{-1}. ESI-MS: *m/z* 726.3 $[M - BF_4^-]^+$. Anal. calcd for $C_{32}H_{54}BF_4FeNiO_3P_2S_2 \cdot 2.25CH_2Cl_2$: C, 40.92; H, 5.87; N, 0.00. Found: C, 40.90; H, 5.82; N, 0.00.

Brown plate-like single crystals of [**3**]$BF_4 \cdot 2CH_2Cl_2$ were grown by layering a concentrated CH_2Cl_2 solution with pentane and allowing the mixture to stand at -28°C. One crystal (0.544×0.295×0.062 mm^3) was subjected to X-ray diffraction at 193 K. Its space group was determined to be monoclinic $P2_1/c$ with cell parameters: a 16.680 Å, b 15.715 Å, c 17.193 Å, α 90.00°, β 92.84°, γ 90.00°. Integration of 3591 reflections and solution by direct methods using SHELXTL V6.12[48,49] afforded a model with R1 = 0.0527 and wR2 = 0.1228.

Phosphine substituted derivatives ([4a-j]BF$_4$)

1 (14.1 mg, 20 μmol) and $FcBF_4$ (5.5 mg, 20 μmol) were dissolved in CH_2Cl_2 (2 mL) with rapid stirring. After 1 min the solution was added dropwise to the appropriate phosphine (200 μmol) in CH_2Cl_2 (0.5 mL). The solution was stirred for a further 0.5 min and pentane (-28°C, 15 mL) was added and the mixture allowed to stand at -28°C for 1 h. The solids were isolated by filtration, washed with pentane (-28°C, 2 × 2 mL) and dried briefly to afford the respective phosphine complexes. The ^{13}CO derivatives were prepared analogously using **1′** as the precursor.

[(dppe)Ni(pdt)Fe(CO)$_2$P(OPh)$_3$]BF$_4$([4a]BF$_4$)

Yield: 78%, yellow-brown powder. ESI-MS: *m/z* 983.9 $[M - BF_4^-]^+$. Anal. calcd for $C_{49}H_{45}BF_4FeNiO_5P_3S_2 \cdot 0.5CH_2Cl_2$: C, 53.33; H, 4.16; N, 0.00. Found: C, 53.41; H, 4.11; N, 0.31.

[(dppe)Ni(pdt)Fe(^{13}CO)$_2$P(OPh)$_3$]BF$_4$([4a′]BF$_4$)

Yield: 70%, yellow-brown powder. ESI-MS: *m/z* 986.0 $[M - BF_4^-]^+$. Anal. calcd for $C_{47}{}^{13}C_2H_{45}BF_4FeNiO_5P_3S_2 \cdot 0.5CH_2Cl_2$: C, 53.24; H, 4.15; N, 0.00. Found: C, 52.97; H, 4.15; N, 0.00.

[(dppe)Ni(pdt)Fe(CO)$_2$P(*p*-C$_6$H$_4$Cl)$_3$]BF$_4$([4b]BF$_4$)

Yield: 87%, yellow-brown powder. ESI-MS: *m/z* 1040.0 $[M - BF_4^-]^+$. Anal. calcd for $C_{49}H_{42}BF_4FeNiO_2P_3S_2Cl_3 \cdot 0.67CH_2Cl_2$: C, 50.36; H, 3.69; N, 0.00. Found: C, 50.49; H, 3.77; N, 0.01.

[(dppe)Ni(pdt)Fe(CO)$_2$PPh$_2$(2-py)]BF$_4$([4c]BF$_4$)

Yield: 80%, yellow-brown powder. ESI-MS: *m/z* 937.1 $[M - BF_4^-]^+$, 908.0 $[M - CO - BF_4^-]^+$. Anal. calcd for $C_{48}H_{44}BF_4FeNiNO_2P_3S_2 \cdot 0.25CH_2Cl_2$: C, 55.38; H, 4.29; N, 1.34. Found: C, 55.30; H, 4.28; N, 1.58.

[(dppe)Ni(pdt)Fe(CO)$_2$PPh$_2$(OEt)]BF$_4$([4d]BF$_4$)

Yield: 81%, yellow-brown powder. ESI-MS: *m/z* 904.0 $[M - BF_4^-]^+$, 567.2 $[M + PPh(OEt) - BF_4^-]^{2+}$. Anal. calcd for $C_{45}H_{45}BF_4FeNiO_3P_3S_2 \cdot 0.25CH_2Cl_2$: C, 53.63; H, 4.53; N, 0.00. Found: C, 53.50; H, 4.74; N, 0.06.

[(dppe)Ni(pdt)Fe(CO)$_2$PPh$_3$]BF$_4$([4e]BF$_4$)

Yield: 93%, yellow-brown powder. ESI-MS: *m/z* 936.3 [M – BF_4^-]$^+$. Anal. calcd for $C_{49}H_{45}BF_4FeNiO_2P_3S_2 \cdot 0.75CH_2Cl_2$: C, 54.92; H, 4.31; N, 0.00. Found: C, 54.70; H, 4.32; N, 0.34.

[(dppe)Ni(pdt)Fe(^{13}CO)$_2$PPh$_3$]BF$_4$([4e′]BF$_4$)

Yield: 73%, yellow-brown powder. ESI-MS: *m/z* 938.0 [M – BF_4^-]$^+$. Anal. calcd for $C_{47}{}^{13}C_2H_{45}BF_4FeNiO_2P_3S_2 \cdot 0.75CH_2Cl_2$: C, 54.82; H, 4.30; N, 0.00. Found: C, 54.70; H, 4.29; N, 0.00.

[(dppe)Ni(pdt)Fe(CO)$_2$PPh$_2$(*o*-C$_6$H$_4$OMe)]BF$_4$([4f]BF$_4$)

Yield: 67%, brown powder. ESI-MS: *m/z* 966.2 [M – BF_4^-]$^+$. Anal. calcd for $C_{50}H_{47}BF_4FeNiO_3P_3S_2 \cdot 0.5CH_2Cl_2$: C, 55.30; H, 4.41; N, 0.00. Found: C, 55.09; H, 4.25; N, 0.38.

[(dppe)Ni(pdt)Fe(CO)$_2$PPh$_2$(*o*-C$_6$H$_4$OCH$_2$OMe)]BF$_4$([4g]BF$_4$)

Yield: 63%, brown powder. ESI-MS: *m/z* 996.4 [M – BF_4^-]$^+$. Anal. calcd for $C_{51}H_{49}BF_4FeNiO_4P_3S_2 \cdot CH_2Cl_2$: C, 53.41; H, 4.40; N, 0.00. Found: C, 53.44; H, 4.35; N, 0.34.

[(dppe)Ni(pdt)Fe(CO)$_2$P(*p*-tol)$_3$]BF$_4$([4h]BF$_4$)

Yield: 89%, yellow-brown powder. ESI-MS: *m/z* 978.3 [M – BF_4^-]$^+$. Anal. calcd for $C_{52}H_{51}BF_4FeNiO_2P_3S_2 \cdot 0.5CH_2Cl_2$: C, 56.87; H, 4.73; N, 0.00. Found: C, 56.58; H, 4.63; N, 0.32.

[(dppe)Ni(pdt)Fe(CO)$_2$P(*p*-C$_6$H$_4$OMe)$_3$]BF$_4$([4i]BF$_4$)

Yield: 96%, yellow-brown powder. ESI-MS: *m/z* 1026.3 [M – BF_4^-]$^+$. Anal. calcd for $C_{52}H_{51}BF_4FeNiO_5P_3S_2 \cdot 0.25CH_2Cl_2$: C, 55.26; H, 4.57; N, 0.00. Found: C, 55.26; H, 4.75; N, 0.25.

[(dppe)Ni(pdt)Fe(CO)$_2$PMePh$_2$]BF$_4$([4j]BF$_4$)

Yield: 76%, brown powder. ESI-MS: *m/z* 874.3 [M – BF_4^-]$^+$. Anal. calcd for $C_{44}H_{43}BF_4FeNiO_2P_3S_2 \cdot CH_2Cl_2$: C, 51.62; H, 4.33; N, 0.00. Found: C, 51.90; H, 4.35; N, 0.23.

[(dppe)Ni(pdt)Fe(CO)$_2$dppe](BF$_4$)$_2$([5](BF$_4$)$_2$)

1 (14.1 mg, 20 μmol) and $FcBF_4$ (10.9 mg, 40 μmol) were partially dissolved in CH_2Cl_2 (2 mL) with rapid stirring. After 1 min the solution was treated dropwise with dppe (8.0 mg, 20 μmol) in CH_2Cl_2 (0.5 mL). The solution was stirred for a further 0.5 min and pentane (-28°C, 15 mL) was added and the mixture allowed to stand at -28°C for 10 min. The solids were isolated by filtration, washed with pentane (-28°C, 2 × 2 mL) and dried briefly to afford the title compound (16.4 mg, 13.2 μmol, 66%) as an orange powder. FT-IR: ν_{CO} = 1967 cm^{-1}. $^{31}P\{^1H\}$ NMR (CD_2Cl_2, 202 MHz) 59.5, 58.3 ppm. Anal. calcd for $C_{57}H_{54}B_2F_8FeNiO_2P_4S_2$: C, 54.89; H, 4.36; N, 0.00. Found: C, 54.77; H, 4.41; N, 0.00.

Orange prismatic single crystals of [**5**]$(BF_4)_2 \cdot 4CH_2Cl_2$ were grown by layering a concentrated CH_2Cl_2 solution with pentane and allowing the mixture to stand at -28°C. One crystal (0.261 × 0.237 × 0.108 mm^3) was subjected to X-ray diffraction at 193 K. Its space group was determined to be triclinic P-1 with cell parameters: a 16.680 Å, b 14.195 Å, c 21.288 Å, α 78.98°, β 75.07°, γ 64.26°. Integration of 9944 reflections and solution by direct

methods using SHELXTL V6.12[48,49] afforded a model with R1 = 0.0465 and wR2 = 0.1126.

Calculations

Calculations of structural parameters and the electronic structure were performed using ORCA.[50] Geometry optimizations were performed using the BP86 exchange-correlation functional[30,31] and a triple-zeta basis set with polarization functions that were obtained from the TURBOMOLE[51] library. In addition, single-point calculations using the hybrid B3LYP[32] and PBE0[33,34] functionals at the BP86/TZVP geometry optimized structures were carried out. This combination of exchange correlation functional and basis set was shown to give accurate structural parameters. IR spectra were generated by numerically calculating second derivatives; calculations of *g*-tensors were performed using an effective mean-field spin-orbit coupling operator, with the center-of-mass as the origin of the *g*-tensor.[52] Additional *g*- and *A*-tensor calculations were performed with ADF[53,54] using the zero order regular approximation (ZORA)[55] for relativistic effects and a self-consistent inclusion of spin-orbit coupling. A Slater-orbital DZ basis set was used for spin-restricted *g*-tensor calculations[56] and a TZP basis set for spin-unrestricted scalar relativistic hyperfine coupling tensor calculations.[57,58]

Supplementary Material

Refer to Web version on PubMed Central for supplementary material.

Acknowledgments

The authors wish to thank Bryan Barton for helpful discussions and Drs. Danielle L. Gray and Amy L. Fuller for X-ray crystallography. This work was supported by the National Institutes of Health (GM061153 to TR, GM46441 and GM084266 to PL).

References

1. Liu T, Darensbourg MY. J. Am. Chem. Soc. 2007; 129:7008. [PubMed: 17497786]
2. Justice AK, De Gioia L, Nilges MJ, Rauchfuss TB, Wilson SR, Zampella G. Inorg. Chem. 2008; 47:7405. [PubMed: 18620387]
3. Justice AK, Nilges M, Rauchfuss TB, Wilson SR, De Gioia L, Zampella G. J. Am. Chem. Soc. 2008; 130:5293. [PubMed: 18341276]
4. Lacey ALD, Fernández VM, Rousset M, Cammack R. Chem. Rev. 2007; 107:4304. [PubMed: 17715982]
5. Ogata H, Lübitz W, Higuchi Y. Dalton Trans. 2009:7577. [PubMed: 19759926]
6. Chapman A, Cammack R, Hatchikian CE, McCracken J, Peisach J. FEBS Lett. 1988; 242:134. [PubMed: 2849556]
7. Whitehead JP, Gurbiel RJ, Bagyinka C, Hoffman BM, Maroney MJ. J. Am. Chem. Soc. 1993; 115:5629.
8. van der Zwaan JW, Albracht SPJ, Fontijn RD, Slater EC. FEBS Lett. 1995; 179:271. [PubMed: 2981705]
9. Stein M, Lubitz W. Phys. Chem. Chem. Phys. 2001; 3:5115.
10. Volbeda A, Charon M-H, Piras C, Hatchikian EC, Frey M, Fontecilla-Camps JC. Nature. 1995; 373:580. [PubMed: 7854413]
11. Volbeda A, Martin L, Cavazza C, Matho M, Faber BW, Roseboom W, Albracht SPJ, Garcin E, Rousset M, Fontecilla-Camps JC. J. Biol. Inorg. Chem. 2005; 10:239. [PubMed: 15803334]
12. Higuchi Y, Ogata H, Miki K, Yasuoka N, Yagi T. Structure. 1999; 7:549. [PubMed: 10378274]
13. Higuchi Y, Yagi T, Yasuoka N. Structure. 1997; 5:1671. [PubMed: 9438867]

14. Matias PM, Soares CM, Saraiva LM, Coelho R, Morais J, Gall JL, Carrondo MA. J. Biol. Inorg. Chem. 2001; 6:63. [PubMed: 11191224]
15. Happe RP, Roseboom W, Pierik AJ, Albracht SPJ, Bagley KA. Nature. 1997; 385:126. [PubMed: 8990114]
16. Tanino S, Li Z, Ohki Y, Tatsumi K. Inorg. Chem. 2009; 48:2358. [PubMed: 19222192]
17. Jiang J, Maruani M, Solaimanzadeh J, Lo W, Koch SA, Millar M. Inorg. Chem. 2009; 48:6359. [PubMed: 20507106]
18. Zhu W, Marr AC, Wang Q, Neese F, Spencer DJE, Blake AJ, Cooke PA, Wilson C, Schröder M. Proc. Natl. Acad. Sci. 2005; 102:18280. [PubMed: 16352727]
19. Barton BE, Whaley CM, Rauchfuss TB, Gray DL. J. Am. Chem. Soc. 2009; 131:6942. [PubMed: 19413314]
20. Barton BE, Rauchfuss TB. J. Am. Chem. Soc. 2010; 132:14877. [PubMed: 20925337]
21. Telser J, Benecky MJ, Adams MWW, Mortenson LE, Hoffman BM. J. Biol. Chem. 1986; 261:13536. [PubMed: 3020036]
22. Carroll ME, Barton BE, Gray DL, Mack AE, Rauchfuss TB. Inorg. Chem. 2011; 50:9554. [PubMed: 21866886]
23. MacNeil JH, Chiverton AC, Fortier S, Baird MC, Hynes RC, Williams AJ, Preston KF, Ziegler T. J. Am. Chem. Soc. 1991; 113:9834.
24. Justice AK, Gioia LD, Nilges MJ, Rauchfuss TB, Wilson SR, Zampella G. Inorg. Chem. 2008; 47:7405. [PubMed: 18620387]
25. Thomas CM, Liu T, Hall MB, Darensbourg MY. Inorg. Chem. 2008; 47:7009. [PubMed: 18597449]
26. Barton BE, Rauchfuss TB. J. Am. Chem. Soc. 2010; 132:14877. [PubMed: 20925337]
27. Tolman CA. Chem. Rev. 1977; 77:313.
28. Bertini L, Greco C, Bruschi M, Fantucci P, Gioia LD. Organometallics. 2010; 29:2013.
29. Liu T, Li B, Singleton ML, Hall MB, Darensbourg MY. J. Am. Chem. Soc. 2009; 131:8296. [PubMed: 19507910]
30. Becke AD. Phys. Rev. A. 1988; 38:3098. [PubMed: 9900728]
31. Perdew JP. Phys. Rev. B. 1986; 33:8822.
32. Stephens PJ, Devlin FJ, Chabalowski CF, Frisch MJ. J. Phys. Chem. 1994; 98:11623.
33. Ernzerhof M, Scuseria G. J. Chem. Phys. 1999; 110:5029.
34. Adamo C, Barone V. J. Chem. Phys. 1999; 110:6158.
35. Redin K, Wilson AD, Newell R, Rakowski DuBois M, DuBois DL. Inorg. Chem. 2007; 46:1268. [PubMed: 17249658]
36. Lubitz W, Reijerse E, van Gastel M. Chem. Rev. 2007; 107:4331. [PubMed: 17845059]
37. Lacey ALD, Stadler C, Fernandez VM, Hatchikian EC, Fan HJ, Li SH, Hall MB. J. Biol. Inorg. Chem. 2002; 7:318. [PubMed: 11935356]
38. van der Zwaan JW, Albracht SPJ, Fontijn RD, Roelofs YBM. Biochim. Biophys. Acta. 1986; 872:208.
39. Pandelia M-E, Ogata H, Currell LJ, Flores M, Lubitz W. Biochim. Biophys. Acta. 2010; 1797:304. [PubMed: 19925776]
40. Pandelia M-E, Ogata H, Lubitz W. ChemPhysChem. 2010; 11:1127. [PubMed: 20301175]
41. Foerster S, Stein M, Brecht M, Ogata H, Higuchi Y, Lubitz W. J. Am. Chem. Soc. 2003; 125:83. [PubMed: 12515509]
42. Bennett B, Lemon BJ, Peters JW. Biochemistry. 2000; 39:7455. [PubMed: 10858294]
43. Popescu CV, Münck E. J. Am. Chem. Soc. 1999; 121:7877.
44. Fiedler AT, Brunold TC. Inorg. Chem. 2005; 44:9322. [PubMed: 16323916]
45. Razavet M, Davies SC, Hughes DL, Barclay JE, Evans DJ, Fairhurst SA, Liu XM, Pickett CJ. J. Chem. Soc., Dalton Trans. 2003:586.
46. Pereira AS, Tavares P, Moura I, Moura JJG, Huynh BH. J. Am. Chem. Soc. 2001; 123:2771. [PubMed: 11456963]

47. Rauchfuss TB. Inorg. Chem. 1977; 16:2966.
48. Sheldrick GM. Acta Cryst. 2008; A64:112.
49. Bruker AXS, I. SHELXTL; Madison, Wisconsin, USA.:
50. Neese, F. ORCA - An ab initio, DFT and semiempirical SCF-MO package, version 2.8.0. University of Bonn; Bonn:
51. Schaefer, A.; Huber, C.; Ahlrichs, R. J. Chem. Phys. 1994. p. 5829http://www.ipc.uni-karlsruhe.de/tch/tch1/index.html
52. Ruud K, Vaara J, Lounila J, Helgaker T. Chem. Phys. Lett. 1998; 297:467.
53. te Velde G, Bickelhaupt FM, van Gisbergen SJA, Guerra CF, Baerends EJ, Snijders JG, Ziegler T. J. Comput. Chem. 2001; 22:931.
54. ADF2010, SCM. Vrije Universiteit; Amsterdam, The Netherlands: Theoretical Chemistry.
55. van Lenthe E, Baerends EJ, Snijders JG. J. Chem. Phys. 1993; 99:4597.
56. van Lenthe E, van der Avoird A, Wormer PES. J. Phys. Chem. 1997; 107:2488.
57. van Lenthe E, van der Avoird A, Wormer PES. J. Chem. Phys. 1998; 108:4783.
58. van Lenthe E, Baerends EJ. J. Chem. Phys. 2000; 112:8279.

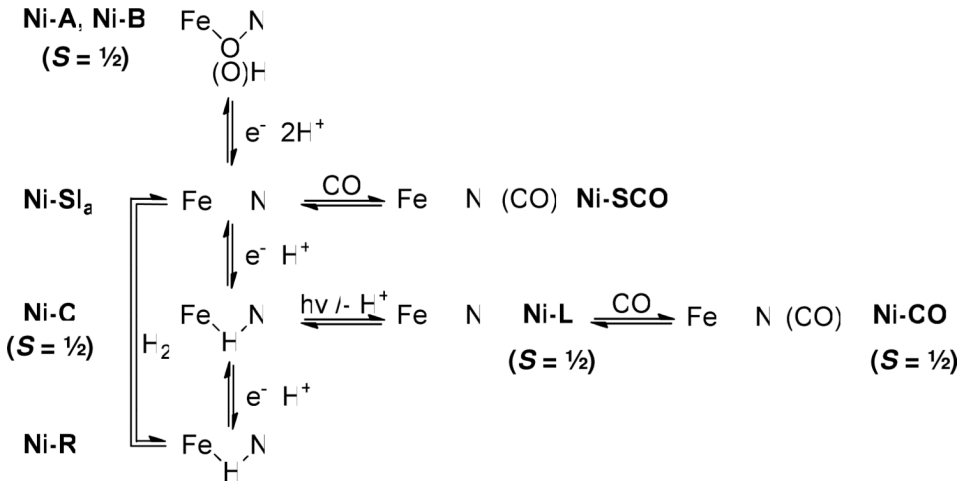

Scheme 1.

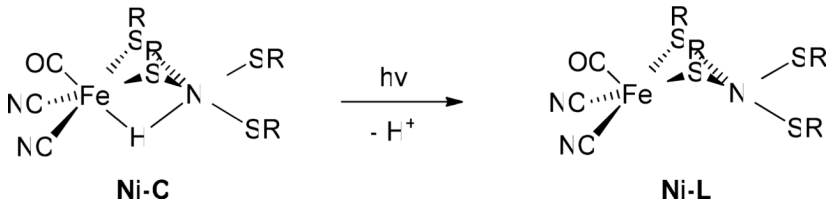

Ni-C **Ni-L**

Scheme 2.

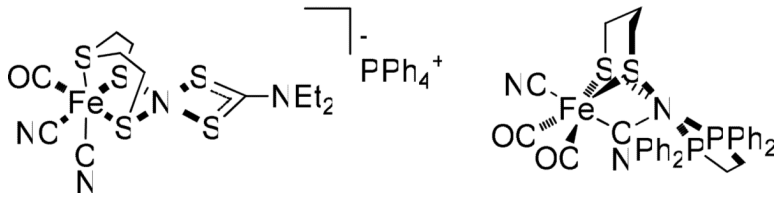

Figure 1.
Structural mimics of the active site of the [NiFe]-H_2ases.

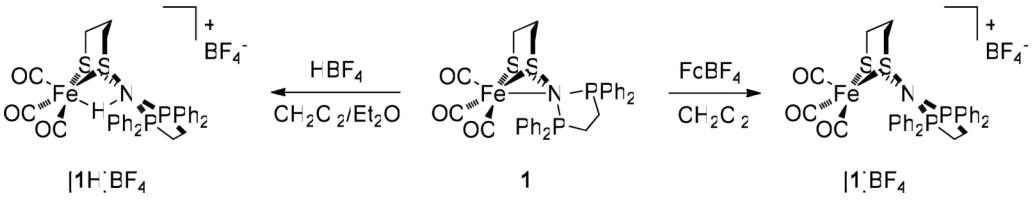

Scheme 3.

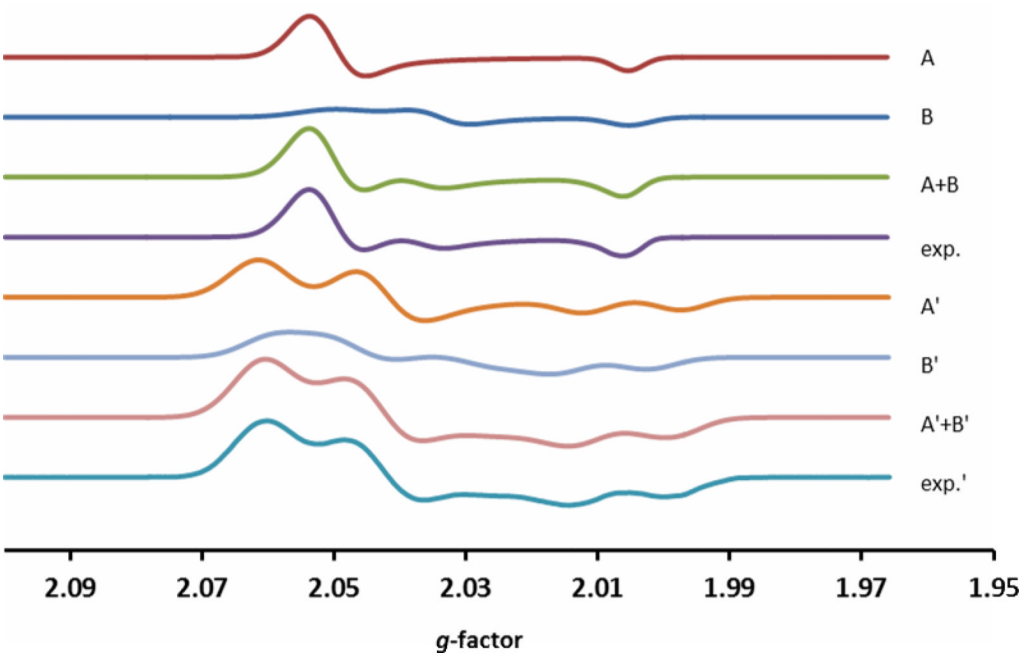

Figure 2.

X-band EPR spectra (CH_2Cl_2/PhMe, 110 K) of [**1**]BF_4 (exp.) and [**1′**]BF_4 (exp.′). In each case the experimental spectrum could be simulated as sum of two components, denoted A+B (for [**1**]BF_4), and A′+B′ (for [**1′**]BF_4).

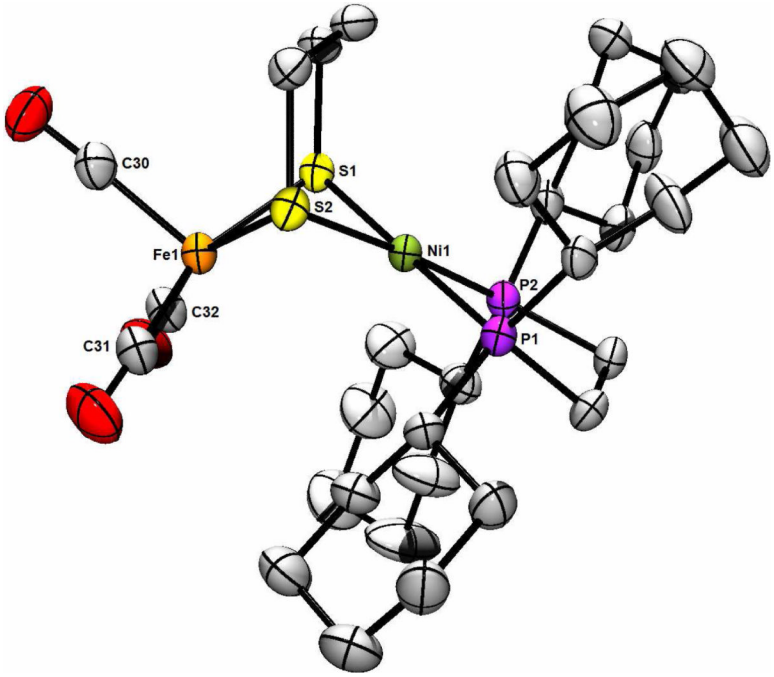

Figure 3.

ORTEP of [**3**]BF_4 with ellipsoids drawn at the 50% probability level. The H atoms, BF_4^- anion, and two CH_2Cl_2 solvate molecules are omitted for clarity. Selected distances (Å): Ni1-Fe1, 2.818; Ni1-P1, 2.191; Ni-P2, 2.188; Ni1-S1, 2.235; Ni1-S2, 2.227; Fe1-S1, 2.296; Fe1-S2, 2.288; Fe1-C30, 1.833; Fe1-C31, 1.799; Fe1-C32, 1.790. Selected calculated (BP/TZVP) distances (Å) Ni1-Fe1, 2.76; Ni1-P1, 2.23; Ni1-P2, 2.22; Ni1-S1, 2.25; Ni1-S2, 2.24; Fe1-S1, 2.31; Fe1-S2, 2.34; Fe1-C30, 1.80; Fe1-C31, 1.79; Fe1-C32, 1.79.

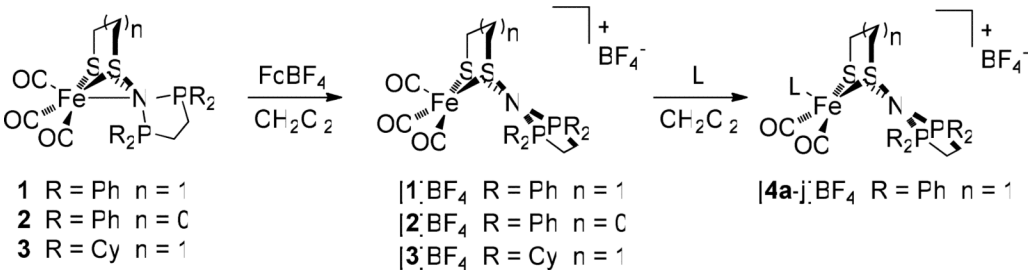

Scheme 4.

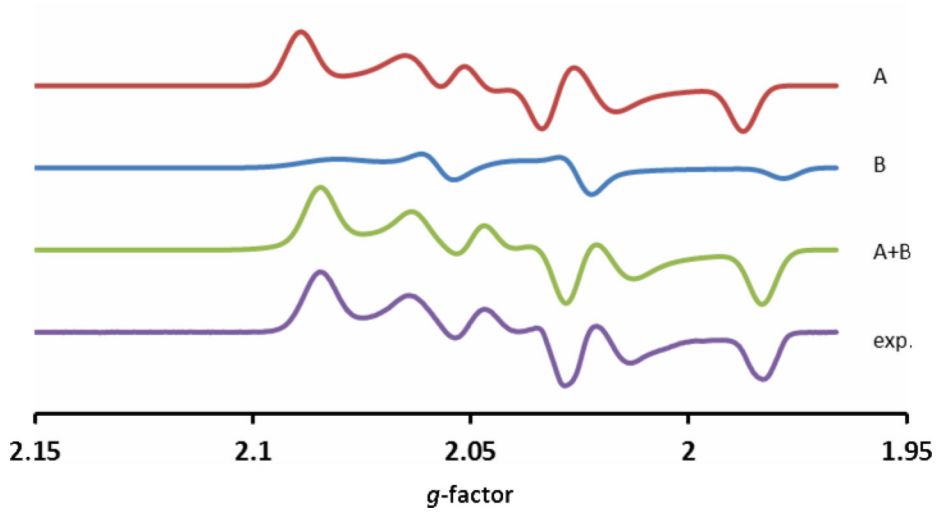

Figure 4.
X-band EPR spectra (CH_2Cl_2/PhMe, 110 K) of [**4e**]BF_4. The experimental spectrum (exp.) could be simulated as sum of two components, denoted A+B.

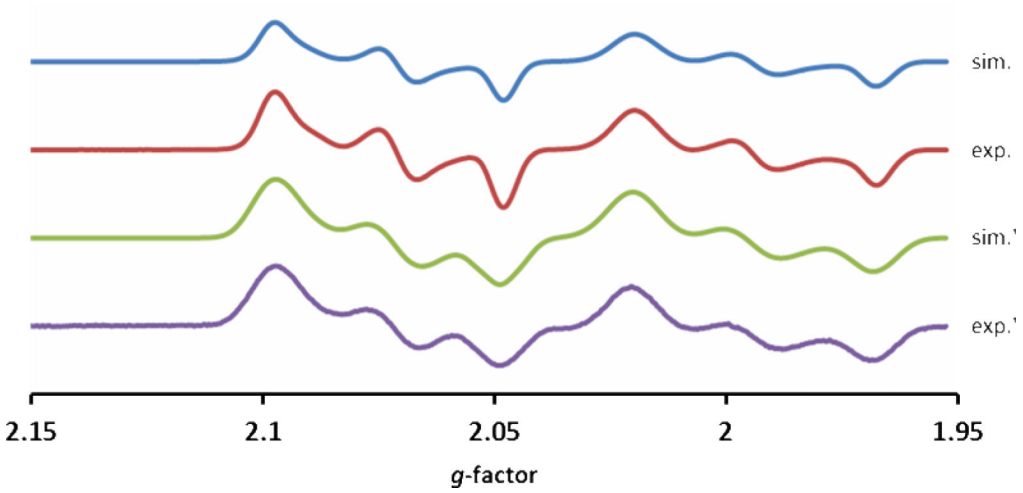

Figure 5.
X-band EPR spectra (CH_2Cl_2/PhMe, 110 K) of [**4a**]BF_4 (exp.) and [**4a′**]BF_4 (exp.′). Simulated spectra (sim. and sim.′, respectively) are also presented.

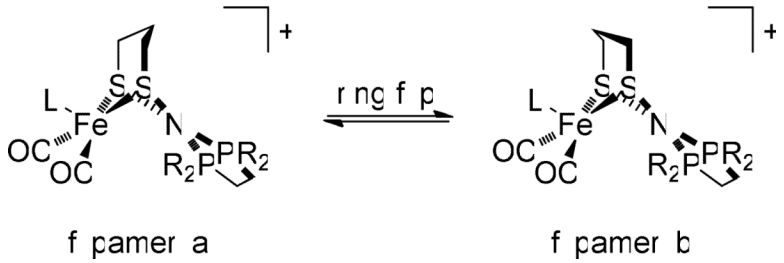

f pamer a f pamer b

Scheme 5.

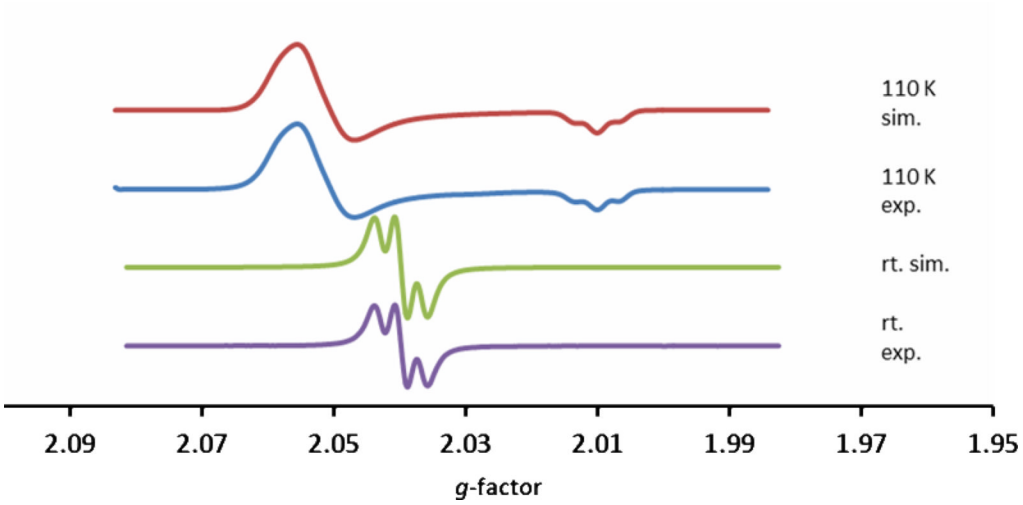

Figure 6.
X-band EPR spectra (CH_2Cl_2/PhMe) of [**2**]BF_4 collected at 110 K (110 K exp.) and room temperature (r.t. exp.). Simulated spectra are also presented.

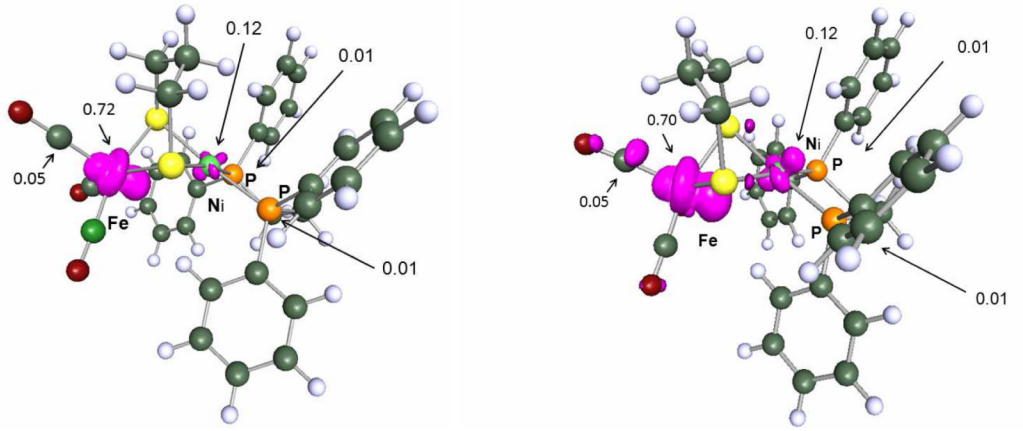

Figure 7.

Isocontour plots of the unpaired spin density distribution at 0.005 e^-/a_0^3 for the two conformers of [**1**]$^+$. The central methylene of the pdt^{2-} ligand can be oriented towards Ni (left, conformer 'a') or Fe (right, conformer 'b'). Unpaired atomic spin densities are given for selected nuclei.

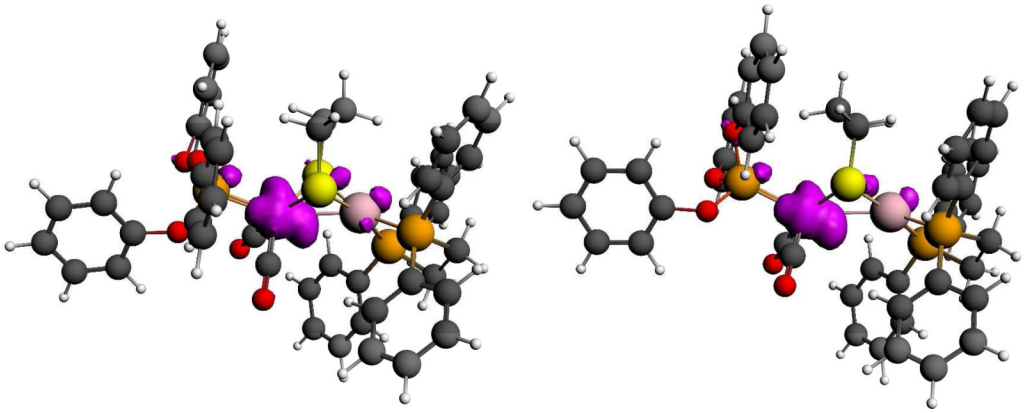

Figure 8.
Isocontour plots of the unpaired spin density distribution at 0.005 e^-/a_0^3 for the two conformers of [**4a**]$^+$. The central methylene of the pdt^{2-} ligand can be oriented towards Ni (left, conformer 'a') or Fe (right, conformer 'b').

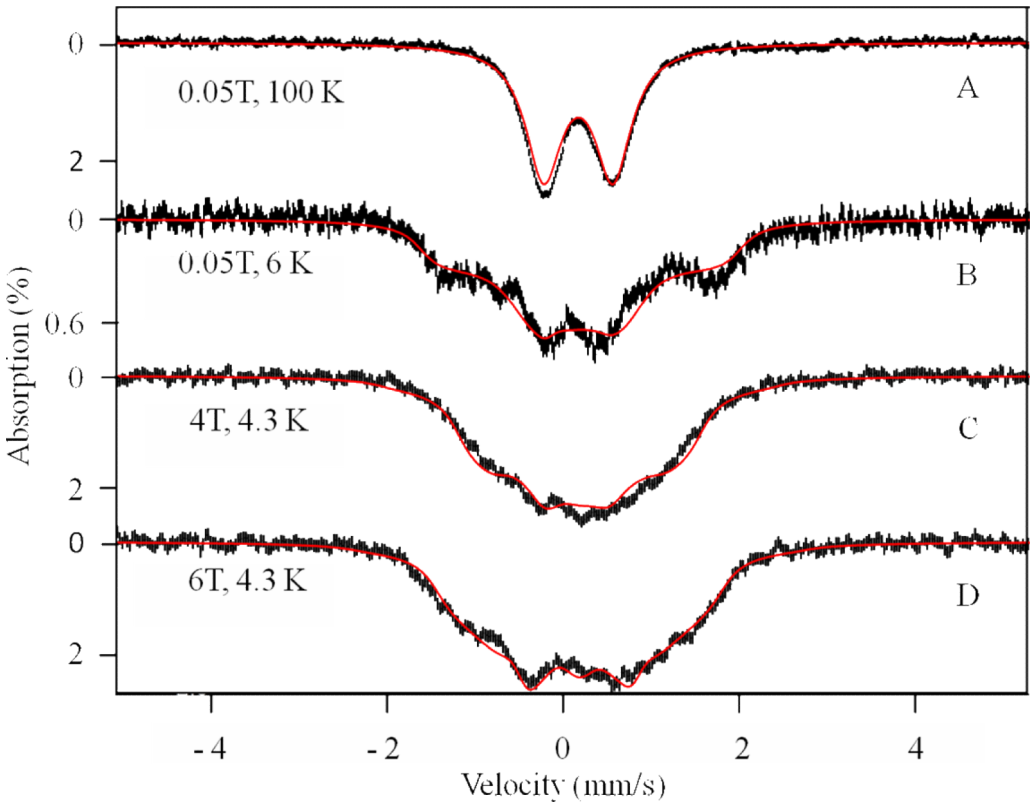

Figure 9.

Mössbauer spectra of [**4e**]BF_4 recorded at the applied fields and temperatures indicated. Spectra A, C and D were obtained on a solid sample while spectrum B was obtained on a 40 mM frozen solution. The magnetic field was parallel to the γ beam for spectra A and B, transverse to the γ beam for spectra C and D. The solid line through the data is a simulation using an S = ½ Hamiltonian with the parameters; δ = 0.18 mm/s, ΔE_Q = 0.79 mm/s, η = 0.7, $A/g_n\beta_n$ = (+ 6.2, -5.5, -28.1) KG, β_{efg} = 45° and γ_{efg} = 90°.

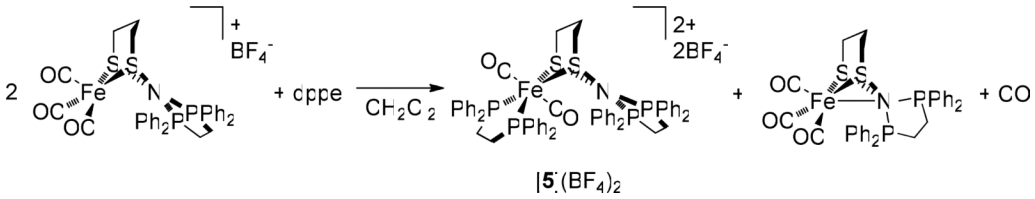

Scheme 6.

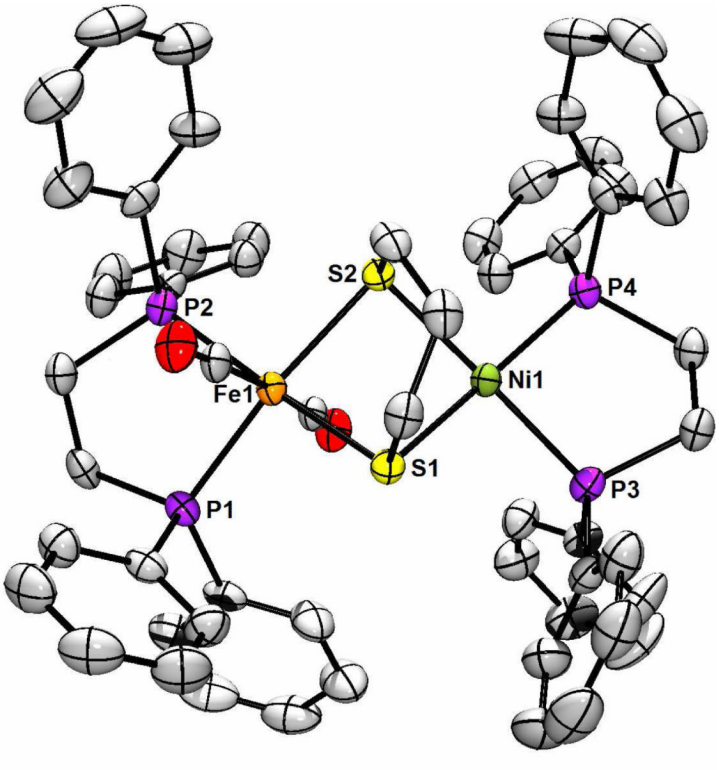

Figure 10.

ORTEP of [**5**]$(BF_4)_2 \cdot 4CH_2Cl_2$ with ellipsoids drawn at the 50% probability level. The H atoms, disordered BF^-_4 anions and four CH_2Cl_2 solvate molecules are omitted for clarity. Selected distances (Å): Ni1-Fe1, 2.818; Fe1-P1, 2.254; Fe1-P2, 2.262; Fe1-C27, 1.800; Fe1-C28, 1.817; Fe1-S1, 2.325; Fe1-S2, 2.334; Ni1-S1, 2.219; Ni1-S2, 2.253; Ni1-P3, 2.186; Ni1-P4, 2.180.

Table 1

IR data for complexes of type [(dppe)Ni(pdt)Fe(CO)$_2$L]BF$_4$ in CH_2Cl_2 solution, ordered in decreasing ν_{CO}. Data for the ^{13}CO-labeled analogs [(dppe)Ni(pdt)Fe(^{13}CO)$_2$L]BF$_4$ are included, these compounds being denoted with prime symbols.

L	Compound	ν_{CO}/cm^{-1}	TEP/cm^{-1}
P(OPh)$_3$	[**4a**]BF$_4$	2007, 1952	2085.3
	[**4a′**]BF$_4$	1961, 1907	
P(*p*-C$_6$H$_4$Cl)$_3$	[**4b**]BF$_4$	1991, 1933	2072.8
PPh$_2$(2-py)	[**4c**]BF$_4$	1990, 1932	
PPh$_2$(OEt)	[**4d**]BF$_4$	1989, 1929	
PPh$_3$	[**4e**]BF$_4$	1988, 1929	2068.9
	[**4e′**]BF$_4$	1941, 1885	
PPh$_2$(*o*-C$_6$H$_4$OMe)	[**4f**]BF$_4$	1987, 1929	2066.1
PPh$_2$(*o*-C$_6$H$_4$OCH$_2$OMe)	[**4g**]BF$_4$	1987, 1928	
P(*p*-tol)$_3$	[**4h**]BF$_4$	1985, 1927	2066.7
P(*p*-C$_6$H$_4$OMe)$_3$	[**4i**]BF$_4$	1985, 1926	2066.1
PMePh$_2$	[**4j**]BF$_4$	1985, 1977, 1928, 1907	2067.1

Table 2

EPR simulation parameters for salts of mixed-valence complexes. Where two entries exist for a given compound, two isomers are represented, the relative abundances of which are given in the last column. Parameters for [**4a**]BF_4 were derived from both X- and Q-band data.

Compound	*g*-factor	$A(^{31}P)$ (MHz)	linewidth (G)	relative abundance
[**1**]BF_4	2.052, 2.050, 2.005		13, 18, 12	0.57
	2.055, 2.038, 2.009		14, 17, 13	0.43
[**1′**]BF_4	2.053, 2.051, 2.005		11, 11, 7	0.62
	2.054, 2.037, 2.008		16, 11, 10	0.38
[**2**]BF_4	2.054, 2.053, 2.010		5, 11, 4	
[**4a**]BF_4	2.058, 2.031, 2.007	345, 345, 364	8, 10, 6	0.68
	2.053, 2.051, 2.004	351, 311, 372	14, 20, 6	0.32
[**4a′**]BF_4	2.058, 2.032, 2.007	345, 345, 364	8, 10, 6	0.68
	2.053, 2.051, 2.004	351, 311, 372	14, 20, 6	0.32
[**4e**]BF_4	2.066, 2.036, 2.006	167, 165, 211	6, 13, 10	0.77
	2.066, 2.045, 2.004	177, 147, 211	22, 5, 11	0.23
[**4e′**]BF_4	2.066, 2.038, 2.006	168, 183, 195	10, 13, 8	0.66
	2.070, 2.042, 2.007	152, 117, 227	12, 20, 6	0.34
[**4h**]BF_4	2.064, 2.036, 2.004	170, 182, 197	11, 13, 8	0.66
	2.069, 2.037, 2.004	147, 122, 228	13, 20, 6	0.34

Table 3

Calculated atomic spin populations (BP/TZVP) for complexes [**1**]$^{+}$, [**2**]$^{+}$, [**3**]$^{+}$, [**4a**]$^{+}$ and [**4e**]$^{+}$.

BP86/TZVP	ρ(Fe)	ρ(Ni)	ρ(P_{dppe})	ρ(apical) C/P
[**1**]$^{+a}$	0.72	0.12	0.01, 0.01	0.05
[**1**]$^{+b}$	0.70	0.12	0.01, 0.01	0.05
[**2**]$^{+}$	0.72	0.12	0.01, 0.01	0.05
[**3**]$^{+a}$	0.71	0.15	0.01, 0.01	0.05
[**3**]$^{+b}$	0.70	0.13	0.01, 0.01	0.06
[**4a**]$^{+a}$	0.71	0.13	0.01, 0.02	0.05
[**4a**]$^{+b}$	0.74	0.11	0.01, 0.01	0.05
[**4e**]$^{+a}$	0.85	0.07	0.01, 0.01	0.06
[**4e**]$^{+b}$	0.86	0.06	0.01, 0.01	0.06